Theodorus Permana[1] and Hiroshi Aoyama[1]

[1] Institute of Seismology and Volcanology, Hokkaido University, Sapporo, Hokkaido, Japan.

Corresponding author: Theodorus Permana (theodorusp@sci.hokudai.ac.jp)

Key Points:

- A seismic source localization method was developed by combining amplitude and delay time information from cross-correlation functions.
- Application to Tokachidake volcano data shows improvements in accuracy than that obtained using only amplitude or delay time information.
- Observed changes in source locations during volcanic tremors and earthquakes suggest volcanic fluid movement towards the crater.

Abstract

Volcanic tremors and earthquakes must be monitored to gain insights into volcanic activity. Localization of their sources is often challenging because of the unclear onset of seismic waves, particularly during an increasing volcanic activity. Existing alternative techniques are based on the information on the spatial amplitude distribution or travel time difference of seismic waves. We propose a new location method that combines both information, obtained from the cross-correlation of seismic data. Evaluation using known volcanic earthquakes at Tokachidake volcano, Japan, reveals some improvements in location accuracy as compared with existing methods using individual information. We further analyze an episode of volcanic tremors and earthquakes accompanying a rapid tilt change event on 14 September 2020. Source locations are mostly distributed at <1 km depth, with evidence of source movement towards the 62-2 crater. Our method is useful in detecting seismic source changes that may represent volcanic fluid migration at shallow depths.

Plain Language Summary

Locating the source of volcanic tremors and earthquakes is important for predicting volcanic eruptions. Common methods use the onset time of earthquakes in seismic recordings, but it is often difficult to observe these onsets. There are alternative methods that use information on either seismic amplitude or delay time at different observation stations. We explored the idea of combining both types of information in a single method, using an analysis called cross-correlation. Tests on known volcanic earthquakes at Tokachidake volcano, Japan, showed some evidence that our method is more accurate than the methods that use only amplitude or delay time. Analysis of an episode of volcanic tremors and earthquakes accompanying the inflation and deflation of the volcano revealed seismic sources at shallow depths that moved towards the crater, reflecting the movement of volcanic fluids beneath the volcano. Our findings demonstrate the usefulness of our method for volcano monitoring.

1. Introduction

Locating the sources of volcanic earthquakes and tremors is an important step in understanding volcanic activity and predicting impending eruptions by studying the movement of volcanic fluids (magma, gas, and water). Conventional methods rely on the onset of seismic phases, which is often difficult to observe during increasing seismicity before or during an eruption. Many studies have used the spatial distribution of seismic amplitudes, hereafter referred to as the "amplitude method", to locate eruption tremors (Battaglia & Aki, 2003; Battaglia et al., 2005; Ichihara & Matsumoto, 2017; Kumagai et al., 2009, 2010; Kurokawa et al., 2016) by comparing observed amplitudes at seismic stations to the theoretical amplitude assuming isotropic radiation of body waves:

$$A_i = A_0 \frac{e^{-Bd_i}}{d_i}, \quad B = \frac{\mathrm{f}}{\mathrm{Q}}, \quad (1)$$

where A_i is the observed amplitude at station i, A_0 is the source amplitude, d_i is the hypocentral distance between the source and station i, f is the representative frequency, Q is the seismic quality factor, and β is the seismic velocity. Terms $1/d$ and e^{-Bd} represent the attenuation of body waves due to geometrical spreading and medium anelasticity, respectively. Estimation of the unknown A_0 can be avoided by computing the ratio of A_i at two stations (Ichihara & Matsumoto, 2017; Taisne et al., 2011; Yamada et al., 2021). Several modifications to the method have also been proposed to address different aspects, such as site amplification factors (Ogiso & Yomogida, 2021).

Another approach to locating seismic events with unclear onsets is using cross-correlation analysis, hereafter referred to as the "cross-correlation method" (e.g., Droznin et al., 2015; Journeau et al., 2020; Permana et al., 2020, 2022). The difference in seismic wave travel time between two stations is represented by the lag (delay) time of the cross-correlation function (CCF) maximum. The observed travel time differences from all possible station pairs then compared with the theoretical ones computed using a known velocity model. Amplitude values are usually ignored by normalizing the seismic data in the time and frequency domains (Bensen et al., 2007), effectively focusing only on the similarity of the wave phases.

Although the amplitude and cross-correlation methods are based on different assumptions and properties of seismic waves, both methods are applied in a limited frequency band and assume a single type of wave (e.g., S-wave) generated by a localized source. The residuals between the observed and theoretical values are examined in various trial source positions using the grid search technique. These similarities provide a possibility of combining amplitude and travel time difference information in a single location method in an attempt to improve location accuracy. For example, Nishimura et al. (2021) separately measured the residuals between the observed and theoretical values for amplitudes and travel

time differences and then computed the total residual. Their method provided better constrains to the source locations compared to those obtained using individual information. In this study, we develop a source location method that uses the amplitude ratio and travel time difference derived from unnormalized CCFs, without separately measuring the residual for each information. We analyze the seismic data of volcanic earthquakes and tremors occurring at Tokachidake volcano in September 2020, where an episode of tilt change, the largest in 2020, was observed. The occurrences of seismic activity and tilt changes indicate volcanic fluids movement at shallow depths. Therefore, locating seismic sources related to such volcanic processes is useful for monitoring the possibility of eruptions. In this study, time information is presented in Japan Standard Time (UTC +9:00).

2. Observation Data

Tokachidake is an active volcano located in the center of Hokkaido, the northernmost major island of Japan, and is being actively and continuously monitored by several agencies. The most recent craters were created during the 1962 eruption, including the 62-2 crater (Figure 1a) where a major explosive episode have occurred during 1988–1989 (Katsui et al., 1990; Okada et al., 1990). In this study, we collected vertical velocity seismograms of 24 known volcanic earthquakes during September 2020 and an episode of volcanic tremors and earthquakes between 08:45 and 10:15 on 14 September 2020 from a network of 12 seismometers consisting of short-period and broadband instruments, with a sampling frequency of 100 Hz (Figure 1a). Three seismometers were installed and maintained by Hokkaido University, eight by the Japan Meteorological Agency (JMA), and one by the National Research Institute of Earth Science and Disaster Resilience (NIED).

In recent times, episodes of increasing volcanic activity have raised concerns regarding the possibility of future eruptions. Volcanic earthquakes are mostly located beneath the 62-2 and Nukkakushi craters as routinely reported by JMA (Japan Meteorological Agency, 2020). The hypocenter distribution of the 24 earthquakes in Figures 1a–b, located by JMA, roughly represents the region of earthquake occurrence at Tokachidake, with durations typically less than 10 s. Volcanic tremors occasionally occur for a duration of approximately 1 min or longer. Tilt changes are sometimes observed accompanying volcanic tremors and earthquakes, indicating source-related processes at shallow depths. On 14 September 2020, an episode of volcanic tremors and earthquakes occurred accompanied by rapid changes in the measured tilt (Figures 1c–d). A 5-min tremor (T1) occurred at 08:51, around which small tilt changes were observed, indicating gradual inflation of the crater area. After T1, the number of volcanic earthquakes (EQ) increased, with the largest ones occurring between 09:06 and 09:24. It is difficult to determine the onset of several earthquakes, as they overlap with each other. At 09:45, a second tremor occurred for 8 minutes (T2), during which the amount and direction of tilt changes rapidly varied until 09:52, when a steep increase was observed. After 09:54, tilt changes started showing

a deflation of the crater area. Several earthquakes and short tremors occurred during this period (aT2). Report by the Japanese Coordinating Committee for Prediction of Volcanic Eruptions (CCPVE) showed that the total amount of tilt change was approximately 2.5 rad, and the tilt change rate during T2 is 23 rad/hour, the largest as compared to that in several previous tilt change episodes in 1–5 November 2019 and 20 January 2020 (Coordinating Committee for Prediction of Volcanic Eruptions, 2020). Increased seismic activity and tilt changes suggest the movement of volcanic fluids beneath the crater area. In this study, we first analyze the 24 volcanic earthquakes with known hypocenters to determine the proper value of input parameters and evaluate the performance of the proposed method. Then, we apply the proposed method to locate the seismic sources during tilt change event.

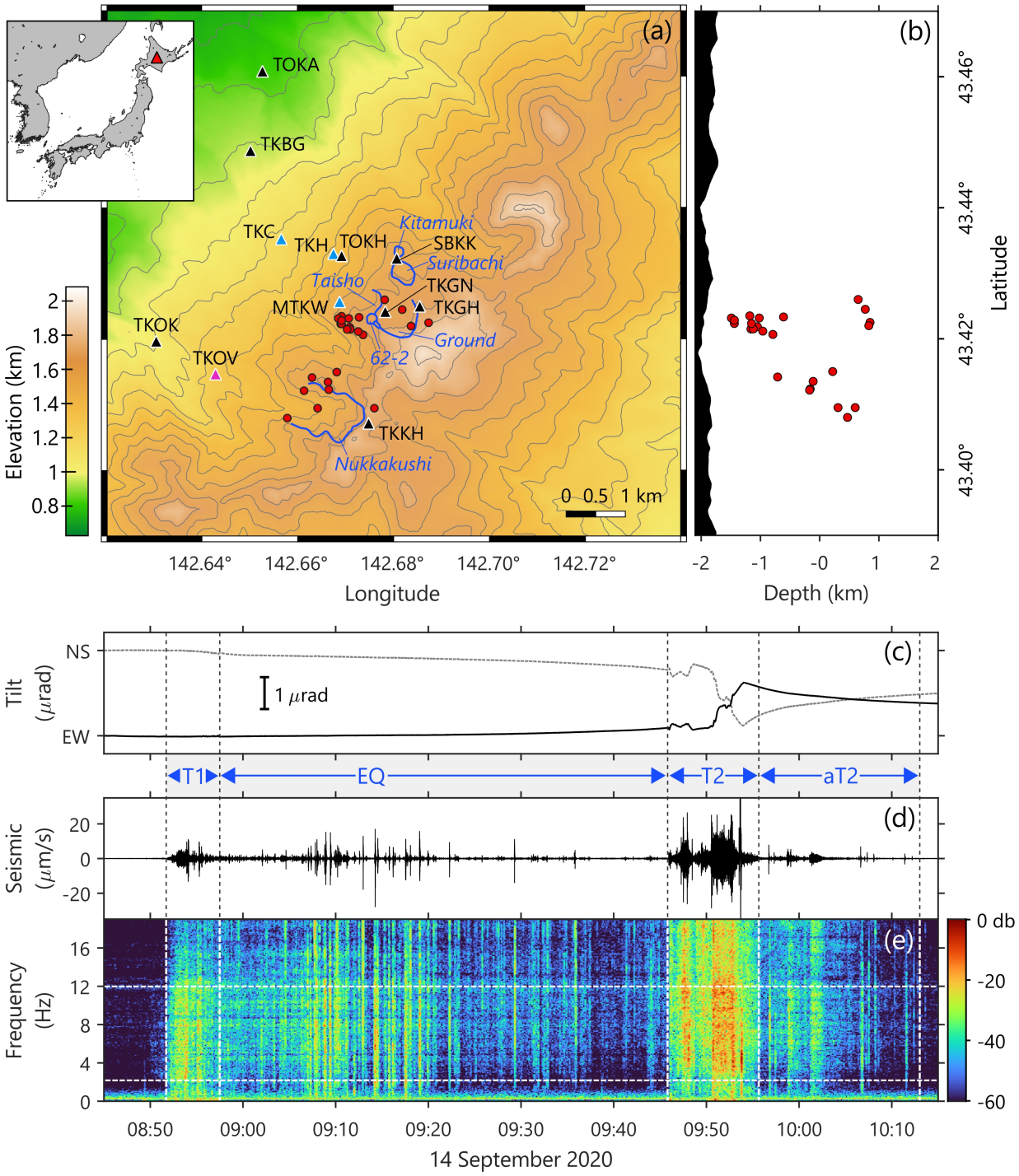
(a)
(b)
(c)
(d)
(e)
TOKA
TKBG
TKC
TKH
TOKH
SBKK
Kitamuki
Suribachi
Taisho
TKGN
TKGH
MTKW
TKOK
TKOV
Ground
62-2
TKKH
Nukkakushi
0 0.5 1 km
Elevation (km)
2
1.8
1.6
1.4
1.2
1
0.8
142.64°
142.66°
142.68°
142.70°
142.72°
Longitude
-2
-1
-0
1
2
Depth (km)
43.46°
43.44°
43.42°
43.40°
Latitude
Tilt (μrad)
NS
EW
1 μrad
T1
EQ
T2
aT2
Seismic (μm/s)
20
0
-20
Frequency (Hz)
16
12
8
4
0
0 db
-20
-40
-60
08:50
09:00
09:10
09:20
09:30
09:40
09:50
10:00
10:10
14 September 2020

Fi

1. Map and observation data of Tokachidake volcano. (a) Elevation map. Blue lines indicate crater outline. Triangles represent seismic stations maintained by Hokkaido University (blue), JMA (black), and NIED (magenta). Red circles denote the hypocenters of 24 volcanic earthquakes in September 2020 determined by JMA. Top left map shows the location of Tokachidake in Japan (red triangle). (b) Depth distribution of volcanic earthquakes. (c) Tilt and (d) vertical seismic velocity at station MTKW during the tilt change event on 14 September 2020. (e) Spectrogram of the seismic waveform. Vertical dashed lines denote the time period of seismic activities T1, EQ, T2, and aT2. Horizontal dashed lines denote the frequency band of 2–12 Hz used in this study.

3. Method

3.1. Development of Source Location Method

In the time domain, cross-correlation is a product of the multiplication and summation of two time-shifted seismograms. Therefore, it is difficult to relate CCF amplitudes to the wave propagation process. However, assuming a very simple case where seismograms at two stations i and j are represented by a single non-zero amplitude of A_i and A_j at the arrival time, respectively (similar to a Dirac delta function), the maximum amplitude of the unnormalized cross-correlation between the two seismograms is equal to $A_i \times A_j$. We assume that A_i and A_j follow equation (1) from a seismic source with an amplitude of A_0. Given cross-correlations from two different station pairs, the ratio of cross-correlation maximum between a station pair of i and j and another station pair of k and l can be theoretically estimated as:

$$\gamma^{\text{the}} = \frac{A_i \times A_j}{A_k \times A_l} = \frac{d_k d_l}{d_i d_j} e^{-B(d_i + d_j - d_k - d_l)}, \quad (2)$$

where the subscripts i, j, k, and l denote station indices. Estimation of A_0 is no longer necessary as in location methods that use the amplitude ratio (Ichihara & Matsumoto, 2017; Taisne et al., 2011).

In the observed seismograms, seismic energy is spread over a longer time period and contains the amplitudes of different seismic phases (e.g., P- and S-waves) at different arrival times. The theoretical ratio γ^{the} holds for general CCFs, assuming that the amplitudes of direct seismic waves from a localized source with a velocity of β are dominant, and the seismograms show similar spectral contents at all seismic stations. We compute the CCFs with no normalization in time or frequency domain beforehand, to retain the physical amplitude information. Then, we compute the CCF smooth envelopes by computing the absolute Hilbert transform and smoothing them using moving average with a specified window length. The peak of the smooth envelopes should be found at the lag time equal to the travel time difference of direct seismic waves from the source, approximated at two station pairs ij and kl as:

$$\tau_{\mathrm{ij}} = T_i - T_j = \frac{d_i - d_j}{\beta}, \quad \tau_{\mathrm{kl}} = T_k - T_l = \frac{d_k - d_l}{\beta}, \quad (3)$$

where T and d are the travel time and distance from the source to the seismic stations, respectively. Then, using the peak amplitude of the CCF envelopes E_{ij} and E_{kl}, we estimate the observed amplitude ratio as:

$$\gamma^{\mathrm{obs}} = \frac{E_{\mathrm{ij}}(\tau_{\mathrm{ij}})}{E_{\mathrm{kl}}(\tau_{\mathrm{kl}})}. \quad (4)$$

Minimization of the residual $\gamma^{\mathrm{obs}} - \gamma^{\mathrm{the}}$ forms the basis of the location method proposed in this study. To estimate an unknown source location, we compute T and d from various trial locations and find the one that minimizes the root-mean-square (RMS) error of residuals:

$$R = \sqrt{\frac{8}{N(N-1)(N-2)(N+1)} \sum_{i=1}^{N-2} \sum_{j=i+1}^{N} \sum_{k=i}^{N-1} \sum_{l=l_0}^{N} \left(\gamma^{\mathrm{obs}} - \gamma^{\mathrm{the}}\right)^2}, \quad (5)$$

j + 1

k + 1

A minimum of three seismic stations are necessary, because the indices i, j, k, and l do not necessarily represent four independent stations. The total number of CCF amplitude ratio values from N available stations is $N(N-1)(N-2)(N+1)/8$. Similar with the amplitude method, we assume isotropic radiation of body waves in a homogeneous medium and measure the distance in 3-D.

3.2. Selection of Parameters Using Known Volcanic Earthquakes

Before applying the proposed method, we first determine the value of the parameters required by the proposed method using the 24 known volcanic earthquakes. Complementary information for this section is provided in Figures S1 and S2 and Table S1 in the Supporting Information. The seismic spectra of volcanic tremors and earthquakes (Figure 1e) show broad frequency contents at >1 Hz. Kumagai et al. (2011) suggested analyzing frequencies of >5 Hz where scattering sufficiently masks the seismic wave radiation pattern and fulfils the isotropic radiation assumption. At such high frequencies, scattered waves may produce wider CCF envelopes (e.g., Permana et al., 2022). We select the frequency band of 2–12 Hz where seismic energy is dominant, especially during tremors, and subsequently use $f = 7$ Hz. We filter the seismograms at the selected frequency band after applying mean removal.

We determine the seismic velocity β and the window length for CCF smooth envelope calculation by computing the smooth envelope from all station pairs using a smoothing window of various lengths (Figure S1c). For each earthquake, we test various velocity values and find the optimum one that minimizes the following RMS error:

$$RMSE = \sqrt{\frac{2}{N(N-1)} \sum_{i}^{N-1} \sum_{j=i+1}^{N} \left(\tau_{max(E_{\mathrm{ij}})} - \tau_{\mathrm{ij}}\right)^2}, \quad (6)$$

where $\tau_{max(E_{\mathrm{ij}})}$ is the lag time of envelope peaks and τ_{ij} is computed from the JMA hypocenter. We average the optimum velocities from all earthquakes as β and compute the standard error. We found that a 2.6 s-long smoothing window produced the smallest error with $\beta = 1.98$ km/s (Figure S1d). This velocity is roughly consistent with S-wave velocities of 1.29–2.36 km/s derived from a P-wave velocity model used by JMA (through division by 1.73) at the depth range of known hypocenters, and within the S-wave velocity range of 1.6–2.7 km/s determined using Rayleigh wave dispersion at 1–3 Hz (Nishimura et al., 1995). Therefore, we assume that S-wave is dominant in the seismic data.

The seismogram must be corrected for local amplification, and the quality factor Q is usually fixed to a reasonable value. In this study, we first compare the observed amplitude decay versus distance with the theoretical value (Equation 1). We obtain the observed amplitudes A_i from the maximum of seismogram envelopes computed using Hilbert transform and smoothed using moving average with a 0.5 s window (Figures S1a–b). We calculate the theoretical amplitude decay versus distance using $\beta = 1.98$ km/s, A_0 estimated following Kumagai et al. (2010), distance d_i measured from the JMA hypocenter, and various Q values. We normalize A_i using A_0 to compare the amplitudes from all earthquakes. We found that the observed amplitude decay can be best explained using $Q = 25$ (Figure S1e). A comparison using other Q values are provided in Figure S2. Then, we compute the amplitude correction factor at station i by assuming that the corrected observed amplitude should be equal to the theoretical amplitude from the JMA hypocenter:

$$s_i = \frac{A_i}{A_0}\ \mathrm{d}_i e^{Bd_i}. \quad (7)$$

Each s_i is computed for all earthquakes and then averaged. The calculated amplitude correction factors for each seismic station are presented in Table S1.

In the following sections, we apply the proposed method to seismic data in 5 s windows to ensure that seismic waves from the largest interstation distance (6.2 km) is captured by cross-correlation. The seismic amplitudes are corrected by dividing the seismogram at each station by the corresponding s_i. We use

only time windows where volcanic signals are well-observed with a signal-to-noise ratio of >10 at six or more stations, where 3-min data prior to T1, from 08:45 to 08:48 on 14 September, is used as the noise window. We apply moving average with a 2.6 s window to obtain CCF smooth envelopes. We evaluate R at each point in a 3-D grid with a resolution of 1 m and determine the optimum source location using $f = 7$ Hz, $\beta = 1.98$ km/s, and $Q = 25$.

4. Results and Discussion

4.1. Source Location of Known Volcanic Earthquakes and Error Estimation

We compare the source locations of volcanic earthquakes determined using the proposed method with those determined with the amplitude method (Kumagai et al., 2010) using the maximum of seismogram envelopes as A_i (see section 3.2) and cross-correlation method (Permana et al., 2020) using CCF envelopes E_{ij} with τ_{ij} for travel time difference estimation. We define location error as the distance of the source location from JMA hypocenter. The JMA hypocenter errors themselves are <75 m in latitude, longitude, and vertical directions and are considered sufficiently accurate as reference locations. The source locations of 15 out of 24 (62.5%) earthquakes show smaller location errors than those of the amplitude and cross-correlation methods (Figures 2a–c), providing proof of improvements in location accuracy as compared with that from other methods. Source locations are generally well located with an error of <0.7 km for earthquakes beneath the 62-2 crater area at >0.5 km elevation. A larger error range of 0.3–3 km is obtained for earthquakes beneath Nukkakushi crater between -0.8 and 0.8 km elevation, where some estimated sources are 1–2 km shallower than the JMA hypocenter. The largest error range of 0.6–4.8 km is obtained for earthquakes beneath 62-2 crater at <0 km depth. Although the errors appear to be larger for deeper earthquakes (Figure 2d), we infer that this inaccuracy is more likely caused by the fact that deeper earthquakes are located outside or around the edges of seismic network coverage. The peak of R distribution for earthquakes around the edges of the seismic network (Figures 2b–c) is broader than that of earthquakes inside the network (Figure 2a), indicating higher uncertainty around the edges of the seismic network. Such inaccuracy is also observed for the amplitude and cross-correlation methods, where the cross-correlation method is the most affected. Installing more stations on the eastern flank of Tokachidake and south of the current network may reduce this location inaccuracy.

We compare the minimum R values obtained for different earthquakes by first normalizing each value using the range of $d_i d_j / d_k d_l$ values computed from the respective source location obtained using the proposed method. We show the location errors as a function of normalized minimum R (R_N^{min}) in Figure 2d. This normalization is also useful for comparing the results from different datasets (e.g., different time windows). The use of the range of $d_i d_j / d_k d_l$ for normalization is a result of trials using different combinations of variables in equation (5) to find the one that provides the most linear relationship with location error (distance from JMA hypocenter), where R_N^{min} should be larger with increasing

error. Therefore, we may develop an empirical approach to estimate the location error of volcanic earthquakes and tremors with no reference locations (i.e., no JMA hypocenters). A linear fitting, shown in Figure 2d, yields an estimation of location error as $2.409R_N^{\min} - 0.202$. For $R_N^{\min}$<0.08 where the estimated error is negative, we simply assume that the source location is highly reliable. We obtain a location error of 1 km (using $R_N^{\min}$ 0.5) for 70% of the earthquakes. In the next section, we apply this empirical error estimation to the source locations of seismic activity during tilt change event.

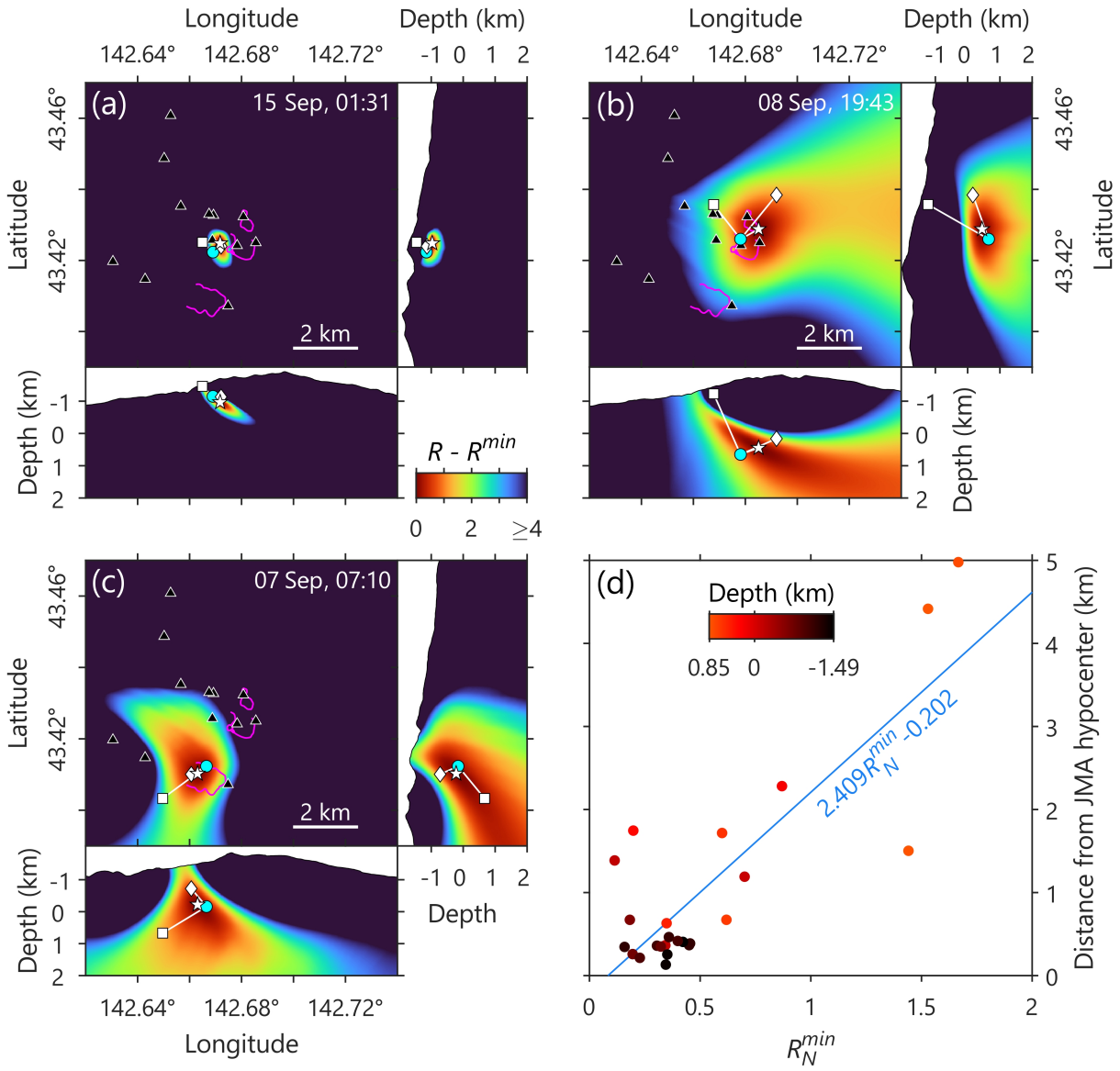

2. Comparison of source locations of volcanic earthquakes in September 2020 and empirical error estimation. (a–c) Distribution of R values for three different earthquakes (colors represent $R - R^{\min}$ values for easier comparison). Circles, squares, diamonds, and stars denote JMA hypocenters and source locations obtained using the cross-correlation, amplitude, and proposed methods, respectively. Triangles represent seismic stations and magenta lines represent crater outlines. (d) Plot of distance between the JMA hypocenter and the source

location obtained using the proposed method (error measure in a–c) versus $R_N^{\min}$. Color represents the focal depth of JMA hypocenters. Blue line shows the linear fit for future location error estimation.

4.2. Source Locations During Rapid Tilt Changes Event

We analyze the seismic data every 5 s during the time period shown in Figure 1d and determine the source location using the proposed method. For comparison, we computed seismic amplitude ratios using two approaches: the ratio of seismogram envelope maximum (see section 3.2) between stations MTKW and TKOV; and the square root of the ratio of CCF envelope maximum from station pairs MTKW–TKGN and TKOV–TKKH. In both approaches, an increase in the amplitude ratio indicates a seismic source that is closer to 62-2 crater area. Figure 3a shows that both amplitude ratios have approximately similar values, where the CCF-based approach reduces short-period large variations in amplitude ratios compared to seismogram-based approach. The amplitude ratios tend to be stable during T1 and EQ and higher during T2 and aT2, suggesting that seismic sources during T2 afterwards are closer to 62-2 crater and possibly shallower.

In general, the estimated source locations are mostly beneath the 62-2 crater area (Figures 3b–d), in approximately the same region as that of volcanic earthquakes located by JMA (Figures 1a–b). Some sources with higher $R_N^{\min}$ values are located further from the 62-2 crater area or outside the seismic network coverage, especially during the EQ time period. We select only source locations with $R_N^{\min}$ of $\leq$0.5 (equivalent to $\leq$1 km error), excluding most of the scattered source locations assumed to be unreliable (Figure 3e). Time windows that are dominated by waves other than S-wave, such as coda waves of earthquakes during EQ, may explain the higher errors. Figures 3f–h show the map of selected source locations. During T1, the sources are located about 1 km southwest of 62-2 crater and gradually migrate closer towards the crater. Vertical locations do not show gradual changes in depth; however, according to the results using known earthquakes, some sources during T1 might be deeper than the located ones, particularly those with larger errors. Sources during T1 and EQ are mostly concentrated between -1 and 0.8 km elevations. These sources tend to be shallower in the later part of EQ during 09:20–09:40, but high variations in vertical locations cause difficulties in observing upward source migration. During T2 and aT2, most sources are more constrained at 0.5–1.3 km elevations or around 0.6 km beneath 62-2 crater.

Analysis of tilt data in volcanic activity report found that the pressure source is shifted from around 1 km depth during T1 to 1.2 km elevation during T2. Gradual inflation between the two tremors indicates source movement towards the crater vicinity (Coordinating Committee for Prediction of Volcanic Eruptions, 2020). These changes in depth are consistent with our seismic source locations, although our seismic sources are distributed between these two pressure sources. It is difficult to compare horizontal location changes because the pressure sources are assumed to be exactly under 62-2 crater. Seismicity at such shallow depths is thought to be generated by hot water and gas from a hydrothermal system

heated by magma at greater depths (Takahashi et al., 2017). T1 may be generated during the period of pressure increase due to fluid movement (Aki & Koyanagi, 1981) towards the conduit at approximately 1 km depth. During EQ, the conduit may have been gradually filled with volcanic fluids, during which the pressure increase continues. The accumulated stress in the surrounding rocks triggers a series of shear faultings, generating the earthquakes. After a brief period of low seismicity, T2 is generated by rapid pressure fluctuations possibly triggered by the fluid-driven crack-forming mechanism of volcanic tremors (Aki et al., 1977) at an elevation of approximately 1 km. An increase in gas bubble formation and its escape from magma below the conduit may further contribute to the rapid increase in pressure. Seismic activity during the deflation of the crater area from the end of T2 may have been caused by degassing and the continuing crack-related processes. Resonance of fluids (Hurst & Sherburn, 1993) at shallow depths beneath 62-2 crater could also explain the short tremors during aT2. There were no significant changes in degassing activity at 62-2 crater and in infrasound signals between the two tremors that might indicate eruptions. In addition, the total amount of observed tilt change during inflation and deflation was approximately the same (Coordinating Committee for Prediction of Volcanic Eruptions, 2020). Therefore, the pressure accumulated since T1 was eventually released without notable changes in surface activities. We may not be able to explain all details of the volcanic processes in this study. Nevertheless, the source locations obtained using the proposed method can provide useful insights into volcanic fluid movement at shallow depths.

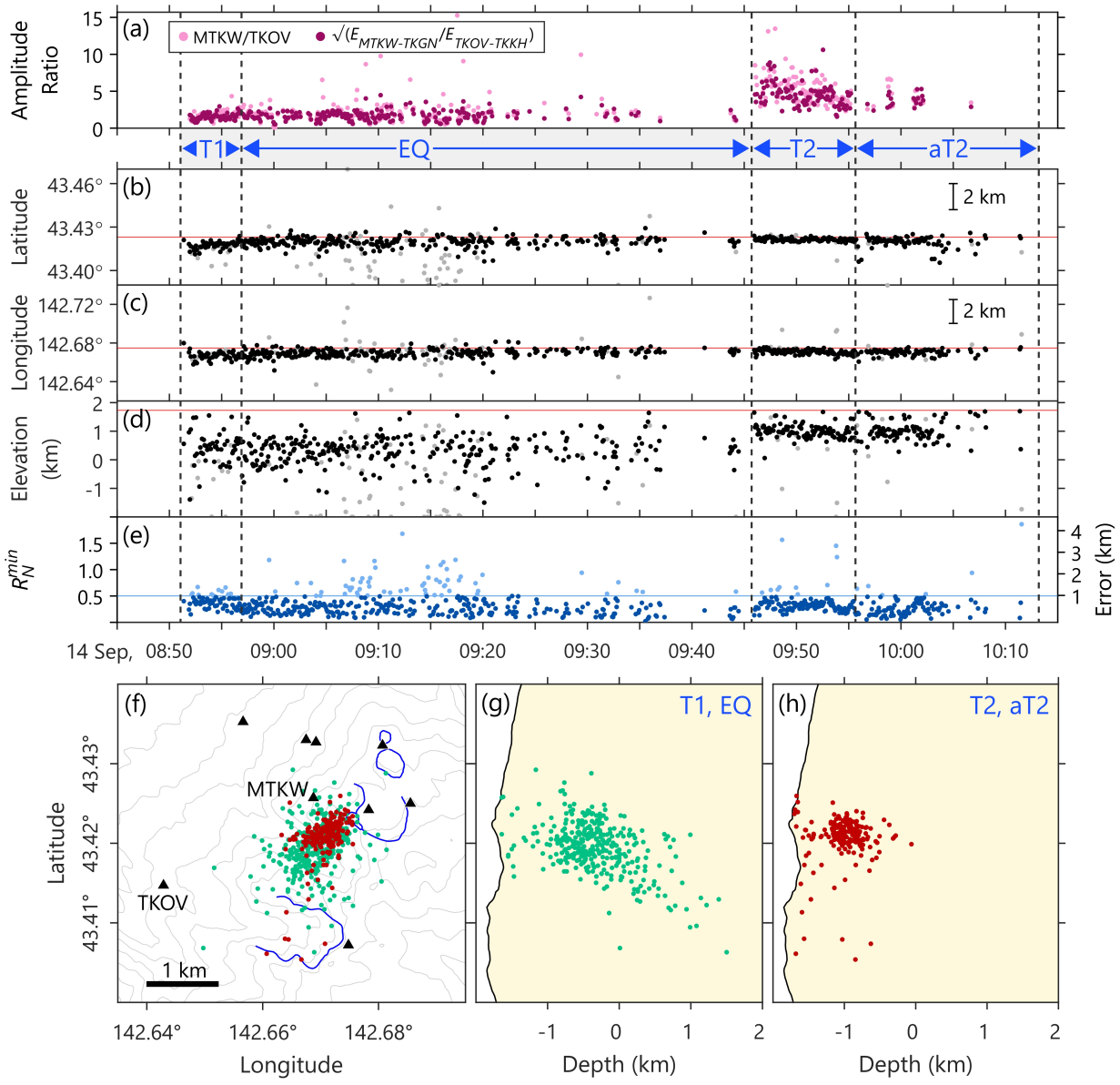

Fi

3. Source locations during rapid tilt changes on 14 September 2020. (a) Amplitude ratios calculated from seismograms (pink circles) and CCFs (purple circles). (b) Latitude, (c) longitude, and (d) elevation of the source locations. Grey circles represent excluded source locations with $R_N^{\min} > 0.5$. Red lines denote the position of 62-2 crater. (e) $R_N^{\min}$ and estimated location errors. Lighter color denotes values larger than the threshold of $R_N^{\min} = 0.5$ (horizontal line). (f) Map of source locations during T1 and EQ (green circles) and during T2 and aT2 (red circles). (g) Depth distribution of the source locations during

T1 and EQ and (h) during T2 and aT2.

5. Conclusions

We developed a method for locating the seismic sources of volcanic tremors and earthquakes using the amplitude and travel time difference information of cross-correlation functions of seismic data recorded at a network of 12 seismic stations in September 2020 at Tokachidake volcano, Japan. Determination of input parameters, method evaluation, and error estimation were performed using data of known volcanic earthquakes, from which we obtained some improvements in location accuracy as compared to that obtained using only amplitudes or travel time differences. Application to an episode of volcanic tremors and earthquakes revealed that seismic source locations with $\leq$1 km of estimated error move towards the 62-2 crater during inflation of the crater area, interpreted as the movement of volcanic gas and hot water. Changes in the depth of source locations were consistent with those from tilt analysis, showing that the proposed method can be useful in volcano monitoring to provide information on volcanic fluid movements beneath the volcano.

Acknowledgments

We thank the JMA and NIED for providing various observational data and the JMA Sapporo Regional Volcanic Observation and Warning Center for providing the catalog of volcanic earthquakes and seismic velocity model at Tokachidake. This study was supported by the Ministry of Education, Culture, Sports, Science and Technology (MEXT) of Japan, under its The Second Earthquake and Volcano Hazards Observation and Research Program (Earthquake and Volcano Hazard Reduction Research). There are no conflicts of interest regarding the content of this paper.

Open Research

Seismic, tilt, and infrasound data from JMA and NIED (https://doi.org/10.17598/NIED.0006) are available through the Data Management Center of NIED at https://www.hinet.bosai.go.jp. Seismic and tilt data from Hokkaido University are provided by the Institute of Seismology and Volcanology (ISV), which are not available to the public because of restrictions concerning data rights and usage policy. Access to those data for research purposes are granted upon request to the ISV (https://www.sci.hokudai.ac.jp/isv/) and agreeing with our data policy. Report on Tokachidake by the CCPVE that were used in this study are available at https://www.data.jma.go.jp/svd/vois/data/tokyo/STOCK/kaisetsu/CCPVE/shiryo/147/147_2-6.pdf (only available in Japanese). JMA report on volcanic activity during 2020 are available at https://www.data.jma.go.jp/svd/vois/data/tokyo/STOCK/monthly_v-act_doc/sapporo/2020y/108_20y.pdf (only available in Japanese). Research report on Tokachidake volcanic system by the Hokkaido Research Organization can be downloaded from https://www.hro.or.jp/list/environmental/research/gs

h/publication/report/gsh_special_report_44.pdf (only available in Japanese). All links and reports were last accessed in April 2022.

References

Aki, K., Fehler, M. & Das, S. (1977). Source mechanism of volcanic tremor: fluid-driven crack models and their application to the 1963 Kilauea eruption. *Journal of Volcanology and Geothermal Research*, *2*(3), 259–287. https://doi.org/10.1016/0377-0273(77)90003-8

Aki, K., & Koyanagi, R. (1981). Deep volcanic tremor and magma ascent mechanism under Kilauea, Hawaii. *Journal of Geophysical Research: Solid Earth*, *86*(B8), 7095–7109. https://doi.org/10.1029/JB086iB08p07095

Battaglia, J., & Aki, K. (2003). Location of seismic events and eruptive fissures on the Piton de la Fournaise volcano using seismic amplitudes. *Journal of Geophysical Research: Solid Earth*, *108*(B8), 2364. https://doi.org/10.1029/2002JB002193

Battaglia, J., Aki, K., & Staudacher, T. (2005). Location of tremor sources and estimation of lava output using tremor source amplitude on the Piton de la Fournaise volcano: 2. Estimation of lava output. *Journal of Volcanology and Geothermal Research*, *147*(3–4), 291–308. https://doi.org/10.1016/j.jvolgeores.2005.04.006

Bensen, G. D., Ritzwoller, M. H., Barmin, M. P., Levshin, A. L., Lin, F., Moschetti, M. P., et al. (2007). Processing seismic ambient noise data to obtain reliable broad-band surface wave dispersion measurements. *Geophysical Journal International*, *169*(3), 1239–1260. https://doi.org/10.1111/j.1365-246X.2007.03374.x

Coordinating Committee for Prediction of Volcanic Eruptions (2020). *The 147th Coordinating Committee for Prediction of Volcanic Eruptions materials (Part 2-6) Tokachidake* (Report No. 147 Part 2-6, only available in Japanese). Retrieved from https://www.data.jma.go.jp/svd/vois/data/tokyo/STOCK/kaisetsu/CCPVE/shiryo/147/147_2-6.pdf

Droznin, D. V., Shapiro, N. M., Droznina, S. Ya., Senyukov, S. L., Chebrov, V. N. & Gordeev, E. I. (2015). Detecting and locating volcanic tremors on the Klyuchevskoy group of volcanoes (Kamchatka) based on correlations of continuous seismic records. *Geophysical Journal International*, *203*(2), 1001–1010. https://doi.org/10.1093/gji/ggv342

Hurst, A. W., & Sherburn, S. (1993). Volcanic tremor at Ruapehu: Characteristics and implications for the resonant source. *New Zealand Journal of Geology and Geophysics*, 36(4), 475-485. https://doi.org/10.1080/00288306.1993.9514593

Ichihara, M., & Matsumoto, S. (2017). Relative source locations of continuous

tremor before and after the subplinian events at Shinmoe-dake, in 2011. *Geophysical Research Letters*, *44*(21), 10,871–10,877. https://doi.org/10.1002/2017GL075293

Japan Meteorological Agency (2020). *Volcanic activity of Tokachidake in Reiwa 2 (2020)* (Report of Sapporo District Meteorological Observatory, Regional Volcanic Observation and Warning Center, only available in Japanese). Retrieved from https://www.data.jma.go.jp/svd/vois/data/tokyo/STOCK/monthly_v-act_doc/sapporo/2020y/108_20y.pdf

Journeau, C., Shapiro, N. M., Seydoux, L., Soubestre, J., Ferrazzini, V., & Peltier, A. (2020). Detection, classification, and location of seismovolcanic signals with multicomponent seismic data: Example from the Piton de la Fournaise volcano (La Réunion, France). *Journal of Geophysical Research: Solid Earth*, *125*(8), e2019JB019333. https://doi.org/10.1029/2019JB019333

Katsui, Y., Kawachi, S., Kondo, Y., Ikeda, Y., Nakagawa, M., Gotoh, Y., et al. (1990). The 1988–1989 explosive eruption of Tokachi-dake, Central Hokkaido, its sequence and mode. *Second Series Bulletin of the Volcanological Society of Japan, 35*(2), 111–129. https://doi.org/10.18940/kazanc.35.2_111

Kumagai, H., Palacios, P., Maeda, M., & Barba, D. (2009). Seismic tracking of lahars using tremor signals. *Journal of Volcanology and Geothermal Research*, *183*(1–2), 112–121. https://doi.org/10.1016/j.jvolgeores.2009.03.010

Kumagai, H., Nakano, M., Maeda, T., Yepes, H., Palacios, P., Ruiz, et al. (2010). Broadband seismic monitoring of active volcanoes using deterministic and stochastic approaches. *Journal of Geophysical Research: Solid Earth*, *115*(B8), B08303. https://doi.org/10.1029/2009JB006889

Kumagai, H., Saito, T., O'Brien, G., & Yamashina, T. (2011). Characterization of scattered seismic wavefields simulated in heterogeneous media with topography. *Journal of Geophysical Research: Solid Earth*, *116*(B3), B03308. https://doi.org/10.1029/2010JB007718

Kurokawa, A., Takeo, M., & Kurita, K. (2016). Two types of volcanic tremor changed with eruption style during 1986 Izu-Oshima eruption. *Journal of Geophysical Research: Solid Earth*, *121*(4), 2727–2736. https://doi.org/10.1002/2015JB012500

National Research Institute for Earth Science and Disaster Resilience (2019). NIED V-net [Dataset], National Research Institute for Earth Science and Disaster Resilience. https://doi.org/10.17598/NIED.0006

Nishimura, T., Hamaguchi, H., & Ueki, S. (1995). Source mechanisms of volcanic tremor and low-frequency earthquakes associated with the 1988–89 eruptive activity of Mt Tokachi, Hokkaido, Japan. *Geophysical Journal International*, *121*(2), 448–458. https://doi.org/10.1111/j.1365-246X.1995.tb05725.x

Nishimura, T., Emoto, K., Nakahara. H., Miura, S., Yamamoto, M., Sugimura, S., et al. (2021). Source location of volcanic earthquakes and subsurface charac-

terization using fiber-optic cable and distributed acoustic sensing system. *Scientific Reports, 11*(1), 6319. https://doi.org/10.1038/s41598-021-85621-8

Ogiso, M., & Yomogida, K. (2021). Estimation of relative source locations from seismic amplitude: application to earthquakes and tremors at Meakandake volcano, eastern Hokkaido, Japan. *Earth, Planets and Space*, *73*(1), 29. https://doi.org/10.1186/s40623-021-01366-8

Okada, H., Nishimura, Y., Miyamachi, M., Mori, H., & Ishihara, K. (1990), Geophysical Significance of the 1988–1989 Explosive Eruptions of Mt. Tokachi, Hokkaido, Japan. *Second Series Bulletin of the Volcanological Society of Japan*, *35*(2), 175–203. https://doi.org/10.18940/kazanc.35.2_175

Permana, T., Nishimura, T., Nakahara, H., Fujita, E., & Ueda, H. (2020). Reliability evaluation of volcanic tremor source location determination using cross-correlation functions. *Geophysical Journal International*, *220*(2), 1300–1315. https://doi.org/10.1093/gji/ggz523

Permana, T., Nishimura, T., Nakahara, H., & Shapiro, M. (2022). Classification of volcanic tremors and earthquakes based on seismic correlation: application at Sakurajima volcano, Japan. *Geophysical Journal International, 229*(2), 1077–1097. https://doi.org/10.1093/gji/ggab517

Taisne, B., Brenguier, F., Shapiro, N. M., & Ferrazzini, V. (2011). Imaging the dynamics of magma propagation using radiated seismic intensity. *Geophysical Research Letters*, *38*(4), L04304. https://doi.org/10.1029/2010GL046068

Takahashi, R., Okazaki, N., Tamura, S., Hashimoto, T., Takahashi, H., Michishita, T., et al. (2017). *Modeling of the internal structure of the volcanic body and the hydrothermal flow system– Advancement of volcanic activity evaluation method (Tokachidake)* (Research Report No. 44 of the Research Institute of Energy, Environment, and Geology, Hokkaido Research Organization, only available in Japanese). Retrieved from https://www.hro.or.jp/list/environmental/research/gsh/publication/report/gsh_special_report_44.pdf

Yamada, T., Kurokawa, A. K., Terada, A., Kanda, W., Ueda, H., Aoyama, H., et al. (2021). Locating hydrothermal fluid injection of the 2018 phreatic eruption at Kusatsu-Shirane volcano with volcanic tremor amplitude. *Earth, Planets and Space*, *73*(1), 14. https://doi.org/10.1186/s40623-020-01349-1